Progress In Electromagnetics Research B, Vol. 36, 35–52, 2012

A NOVEL WAVELET-GALERKIN METHOD FOR MODELING RADIO WAVE PROPAGATION IN TROPOSPHERIC DUCTS

A. Iqbal* **and V. Jeoti**

Department of Electrical and Electronics Engineering, Universiti Teknologi PETRONAS, Tronoh, Perak 31750, Malaysia

Abstract—In this paper, a novel Wavelet-Galerkin Method (WGM) is presented to model the radio-wave propagation in tropospheric ducts. Galerkin method, with Daubechies scaling functions, is used to discretize the height operator. Later, a marching algorithm is developed using Crank-Nicolson (CN) method. A new "fictitious domain method" is also developed for parabolic wave equation to incorporate the impedance boundary conditions in WGM. In the end, results are compared with those from Advance Refractive Effects Prediction System (AREPS). Results show that the wavelet based methods are indeed feasible to model the radio wave propagation in troposphere as accurately as AREPS and proposed method can be a good alternative to other conventional methods.

1. INTRODUCTION

Parabolic Wave Equation (PWE) method is a widely used technique for modeling tropospheric anomalous radio wave propagation. To date, several numerical techniques have been developed to solve PWE. However, the most popular among them is the Split-Step Fourier transform Method (SSFM) [1]. Though it is quite popular among researchers, this algorithm is not effective for modeling arbitrary boundary conditions. An important advancement in this technique is the introduction of the Discrete Mixed Fourier Transform (DMFT) [2]. DMFT based SSFM allows one to handle finitely conductive surfaces. Finite Difference Method (FDM) is considered effective for all types of boundary conditions [1]. But for non-standard atmosphere or

Received 12 September 2011, Accepted 27 October 2011, Scheduled 3 November 2011
* Corresponding author: Asif Iqbal (asif.iqbal@msn.com).

complex refractive structure, the matrices become more and more dense. So, it takes long to solve these matrices and it also uses up too much memory. Finite Element Method (FEM) has also been employed for the solution of parabolic equation [3–7]. Effective boundary handling makes FEM attractive to numerical solution of partial differential equations (PDE). Recently, Apaydin and Sevgi [8] extended the solution for the application to surface wave propagation. But in their work, modified refractivity is assumed linear which is not a suitable assumption for higher frequencies. From literature review, it is also found that the finite methods developed so far are accurate only up to the maximum of second order. To handle singularities and abnormal environment, higher order methods are not only computationally more efficient but also more accurate. Advance Refractive Effects Prediction System (AREPS) software is used as a benchmark in this work, because it is optimized for tropospheric radio-wave propagation modeling and considered to be most suitable software package. The Advance Propagation Method (APM) is the core of AREPS. APM is a hybrid model which contains four models. These are flat earth (FE), ray optics (RO), extended optics (XO), and the Split-Step Parabolic Equation (PE) Algorithm. PE Method is the primary model around which the other three sub-models are built [9].

In this work, a novel more accurate WGM is presented to model radiowave propagation in troposphere. Wavelet based numerical methods are most often used to solve linear and non-linear differential equations [10–14]. Orthogonality, compact support and exact representation of polynomials of a fixed degree make them useful for representing the solutions of PDEs. According to the best of authors' knowledge, application of wavelets to model radio wave propagation is not addressed in literature so far. In the formulation of WGM, Daubechies scaling functions are used as basis functions in Galerkin method to solve 2D PWE. The discretization process is applied to height operator. Resultant system of algebraic equations is solved by CN Method. In this paper, a new fictitious domain method based on Lu et al. [15] is also developed for parabolic equations to handle arbitrary boundary conditions without losing the simplicity of WGM. Parametric refractivity M-profile model is used to generate vertically modified refractivity profile to mimic real environment [16]. The proposed method not only provides higher order accurate solution, it can also handle any type of ducting profile.

The rest of the paper is organized as follows: Brief background of radio refractive index, an overview of PWE and Basic Wavelet theory is given in Section 2. Detailed WGM formulation is described in Section 3. In Section 4, numerical implementation of WGM along

with fictitious domain method is presented. Results comparison and discussion is provided in Section 5.

2. BACKGROUND

2.1. Radio Refractive Index

The radio refractive index (n) is caused due to the molecular constituents of the air [17]. Normally, the numerical difference in refractivity is a very small fraction of unity. So, a convenient way of expressing the refractive index is in terms of refractivity (N) is given by,

$$N = (n-1) \times 10^6 \tag{1}$$

There are four refractive conditions which depend upon refractive gradient. The relations of refractivity gradient and related refractive condition are summarized in Table 1 [18]. Trapping condition, often called ducting phenomenon, causes anomalous radiowave propagation. Well known tropospheric ducts are surface duct (ground-based duct), surface-based duct and elevated duct as shown in Figure 1.

2.2. Parabolic Wave Equation (PWE)

A two dimensional scalar wave equation in the cartesian coordinates system can be written as:

$$\frac{\partial^2 \psi}{\partial x^2} + \frac{\partial^2 \psi}{\partial z^2} + k^2 n^2 \psi = 0. \tag{2}$$

In the equation mentioned above, $k = 2\pi/\lambda$ is the wave number in vacuum, and n is the refractive index. To reduce (2) into PWE, a function associated with the paraxial direction x is taken as [1],

$$\psi(x, z) = u(x, z) e^{jkx} \tag{3}$$

Table 1. Refractive condition.

Condition	**N-Gradient** (N — Unit/km)	**M-Gradient** (M — Unit/km)
Trapping	$dN/dh \leq -157$	$dM/dh \leq 0$
Supper Refraction	$-157 < dN/dh \leq -79$	$0 < dM/dh \leq 78$
Standard	$-79 < dN/dh \leq 0$	$78 < dM/dh \leq 157$
Sub Refraction	$dN/dh > 0$	$dM/dh > 78$

Substituting (3) into (2) we obtain

$$\frac{\partial^2 u}{\partial x^2} - 2jk\frac{\partial u}{\partial x} + \frac{\partial^2 u}{\partial z^2} + k^2\left(n^2 - 1\right)u = 0 \tag{4}$$

Using paraxial approximation, i.e., $\partial^2 u/\partial x^2 \ll 2jk\partial u/\partial x$, (4) will be reduced to the familiar PWE in two-dimensional space:

$$\frac{\partial^2 u}{\partial z^2} - 2jk\frac{\partial u}{\partial x} + k^2\left(n^2 - 1\right)u = 0 \tag{5}$$

This is called standard parabolic equation (SPE). For Earth flattening, the factor $(n^2 - 1)$ in (5) should be replaced by $(n^2 - 1 + 2z/R)$ [8], where, R is the Earth's Radius and z the height above the ground level.

2.3. Boundary Conditions

2.3.1. Impedance Boundary Conditions

With the assumption that the skin depth of electromagnetic radiation within the earth is small as compared to the earth's radius of curvature, the boundary conditions (BC) at smooth earth surface can be approximated by [2]:

$$\alpha_1(x)\frac{\partial}{\partial z}u(x,z)|_{z=0} + \alpha_2(x)u(x,z)|_{z=0} = 0 \tag{6}$$

where, $\alpha_1(x)$ and $\alpha_2(x)$ are constants. For a perfectly conducting surface, $\alpha_1(x) = 0$ (Dirichlet BC) and $\alpha_2(x) = 0$ (Neumann BC) for horizontal and vertical polarization respectively. For finitely conducting earth surface, $\alpha_1(x) = 1$, while $\alpha_2(x) = (j/\mu_0\omega)\eta$ for

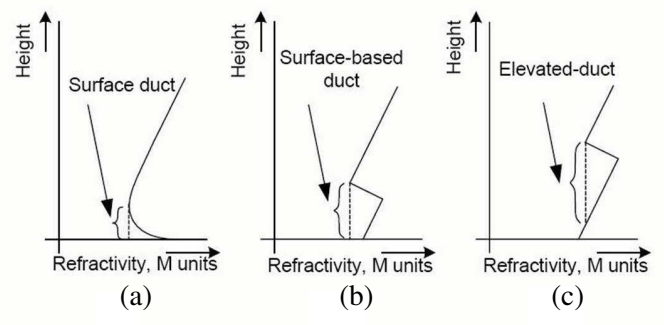

Figure 1. Type of Ducts. (a) Surface duct. (b) Surface-based duct. (c) Elevated duct.

horizontal polarization and $\alpha_2(x) = -j\omega\varepsilon_s\eta$ for vertical polarization, where ε_s is the permittivity of the surface medium, μ_0 the free-space permeability, and ω the radial frequency.

2.3.2. Absorbing Boundary Conditions

In order to limit the height of computational domain there is a need to truncate the domain at finite height. Artificial truncation can cause strong reflections. To avoid these non-physical reflections, a windowing function, perfectly matched layer (PML) termination, or locating an absorbing layer is used [1, 8, 19]. In this paper, a windowing function is used as an absorbing layer.

2.4. Initial Field

PWE is an initial value problem. It is necessary to specify the field at range $x = 0$. There are several ways that the starting field can be generated, e.g., by some analytical function or by using antenna theory. The field at range $x = 0$ is essentially the antenna aperture distribution, and the far-field antenna pattern $f(p)$ and its aperture distribution $A(z)$ are a Fourier transform pair [9],

$$A(z) \overset{\mathfrak{F}}{\rightarrow} f(p) \tag{7}$$

where $\mathfrak{F}$ is Fourier transform. Applying the boundary condition that the field vanishes at the surface, we use image theory to obtain:

$$\psi(0, z) = A(z - z_0) + \Gamma \cdot A^*(z + z_0) \tag{8}$$

where Γ is the reflection coefficient. Equation (8) is written as the sum of the source and image fields, and z_0 represents the antenna height. Since the antenna pattern is what is normally dealt with, one can simply transform it to obtain

$$\tilde{\psi}(0, p) = f(p)e^{-jpz_0} + \Gamma \cdot f^*(p)e^{-jpz_0} \tag{9}$$

Pattern factor $f(p)$ for omnidirectional antenna is equal to 1, and for a normalized Gaussian antenna pattern:

$$f(p) = e^{-p^2w^2/4}, \quad \text{where} \quad w = \sqrt{2\ln 2}/k_0 \sin(\theta_{bw}/2) \tag{10}$$

In (10), $\theta_{bw}/2$ is beam-width angle. Elevation angle can easily be incorporated by replacing $f(p)$ by $f(p - p_0)$. Where $p_0 = k_0 \sin\theta_0$.

2.5. Basic Wavelet Theory

Ingrid Daubechies constructed the class of compactly supported scaling and wavelet function in 1988 [20]. Briefly, scaling function (φ) satisfies the following expression, called Dilation Equation:

$$\varphi(z) = \sum_{k=0}^{M-1} h_k \varphi(2z - k)$$

where M is the order of Daubechies wavelet, and $\varphi(z)$ is called scaling function. The associated wavelet function ψ is required to satisfy the following equation called wavelet equation:

$$\psi(z) = \sum_{k=-1}^{M-2} (-1)^k h_{k+1} \varphi(2z + k)$$

where h_k is the set of nonzero constant scaling coefficients with condition

$$\sum_{k=0}^{M-1} h_k = 2$$

The orthogonal wavelet and scaling functions generated with these scaling coefficients will have a $\text{supp}(\varphi) = [0, M-1]$. For $j,\ k \in \mathbb{Z}$, the dilation and translations of scaling function ($\varphi(z)$) and wavelet function ($\psi(z)$) can be written as:

$$\varphi_{j,k}(z) = 2^{j/2} \varphi\left(2^j z - k\right)$$
$$\psi_{j,k}(z) = 2^{j/2} \psi\left(2^j z - k\right)$$

Let V be the set of all scaling functions and W the set of all wavelet functions. A brief summary of wavelet properties is given as follows. For more details, see [20–22].

(1) $\{\varphi_{j,k}\}_{j \geq 0, k \in \mathbb{Z}}$ is an orthonormal basis for $L^2(\mathbb{R})$.
(2) $V_{j+1} = V_j \oplus W_j$.
(3) $L^2(\mathbb{R}) = \text{clos}_{L^2}(V_0 \oplus_{j=0}^{\infty} W_j)$.
(4) $\{\varphi_{0,k}, \psi_{j,k}\}_{j \geq 0, k \in \mathbb{Z}}$ is an orthonormal basis for $L^2(\mathbb{R})$.
(5) $\int_{-\infty}^{\infty} \varphi(z) dz = 1$.
(6) $\sum_{k \in \mathbb{Z}} \varphi_{0,k} = 1$.
(7) $\int_{-\infty}^{\infty} \psi(z) z^k dz = 0$: $k = 0, \ldots, L-1$.
(8) $\{z^k\}_{k=0}^{L-1} \in V_N$, where L is an positive integer.

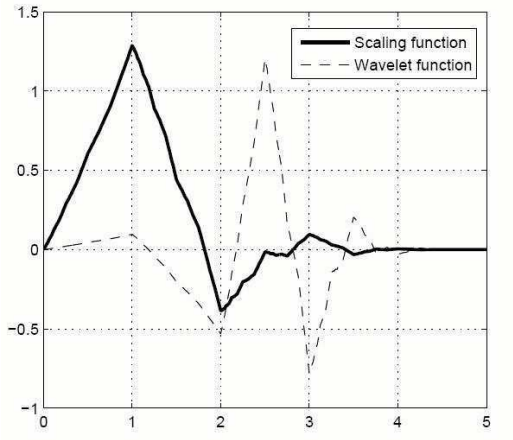

Figure 2. Daubechies scaling and wavelet function for $M = 6$ with support [0, 5].

Based on property (2), the multiresolution analysis is a nested sequence,

$$V_0 \subset V_1 \subset \ldots \subset L^2(\mathbb{R})$$

satisfying the following properties [22].

(1) $\bigcap_{j\in\mathbb{Z}} V_j = 0$

(2) $\text{clos}_{L^2}(\bigcup_{j\in\mathbb{Z}} V_j) = L^2(\mathbb{R})$.

(3) $f(z) \in V_j \Leftrightarrow f(2z) \in V_{j+1}$.

(4) There is a function $\varphi \in V_0$ such that $\{\varphi_{0,k}(z) = \varphi(z-k)\}$ form a Riesz basis for V_0.

For arbitrarily large even M, the Daubechies family of wavelet have fundamental support in the interval $[0,\ M-1]$. In Figure 2 an example of a compactly supported Daubechies scaling and wavelet functions for $M = 6$ are shown.

3. WAVELET GALERKIN METHOD (WGM)

Solution domain is divided into several subdomains in WGM. The approximate solution is written in the form of,

$$f(z) = \sum_{l=1}^{N_z} f_l \varphi_l(z) \tag{11}$$

where N_z is number of grid points, f_l the unknown coefficients, and φ_l the wavelet scaling basis functions. Inner product of basis functions can be defined as,

$$\langle \varphi_k, \varphi_l \rangle = \int_{-\infty}^{\infty} \varphi_k \varphi_l dz \tag{12}$$

Inner product of wavelet scaling basis functions with or without derivatives is called connection coefficients. Connection coefficients for unbounded intervals were described by Latto et al. [23]. In General form, n-term connection coefficients can be defined as

$$\Omega_{k_1,\ldots,k_n}^{d_1,\ldots,d_n} = \int_{-\infty}^{\infty} \varphi_{k_1}^{d_1} \ldots \varphi_{k_n}^{d_n} dz = \int_{-\infty}^{\infty} \prod_{i=1}^{n} \varphi_{k_i}^{d_i} dz \tag{13}$$

where superscript d_i refers to the derivative of the scaling function $\varphi(z)$ with respect to z. If the discretizing operator is linear, then integral will have the form as hereunder,

$$\Omega_{k,l}^{d_1,d_2} = \int_{-\infty}^{\infty} \varphi_k^{d_1} \varphi_l^{d_2} dz \tag{14}$$

here, $\Omega_{k,l}^{d_1,d_2}$ is known as 2-term connection coefficients. In the formulation of PWE, maximum of 2-term connection coefficient will be used. By change of variable, 2-term connection coefficient $\Omega_{k,l}^{d_1,d_2}$ can be turned into $\Omega_{0,l-k}^{d_1,d_2} := \Omega_{0,l'}^{d_1,d_2}$, where $l' = l - k$. For simplicity, $\Omega_{l}^{d_1,d_2}$ will be used throughout this document,

$$\Omega_{l}^{d_1,d_2} = \int_{-\infty}^{\infty} \varphi^{d_1} \varphi_l^{d_2} dz \tag{15}$$

More details can be found in [23, 24].

3.1. WGM Formulation for PWE

In the formulation of WGM, weak form of (5) can be obtained by multiplying (5) with basis function φ_k and integrating over the domain:

$$\int \varphi_k \left(\frac{\partial^2 u}{\partial z^2} - 2jk \frac{\partial u}{\partial x} + k^2 \left(n^2 - 1 \right) u \right) dz = 0 \tag{16}$$

In discrete space,

$$u(x, z) = \sum_{l} a_l(x) \varphi_l(z) \tag{17}$$

where,

$$a_l = \langle u(x, z), \varphi_l \rangle$$

After substituting the wavelet expansion of $u(x,z)$ into (16) and rearranging, we have

$$\sum_l a_l'(x)\int \varphi_k\varphi_l dz + \sum_l a_l(x)\left(\frac{j}{2k}\int \varphi_k\varphi_l'' dz - \frac{jk}{2}\left(k^2(n^2-1)\right)\int \varphi_k\varphi_l dz\right) = 0 \tag{18}$$

In matrix notations, (18) can be written as

$$[\delta_{k,l}]\{a_l'(x)\} + [L_{k,l} + S_{k,l}]\{a_l(x)\} = 0 \tag{19}$$

where,

$$\delta_{k,l} = I_{k,l} = \int \varphi_k\varphi_l dz,$$

$$L_{k,l} = \frac{j}{2k}\int \varphi_k\varphi_l'' dz = \frac{j}{2k}\left(\Omega_l^{0,2}\right),$$

$$S_{k,l} = -\frac{jk}{2}\left(k^2(n^2-1)\right)\int \varphi_k\varphi_l dz,$$

$\delta_{k,l}$ is known as Kronecker delta function, and $\Omega_l^{0,2}$ are the connection coefficient briefly described in previous section. If whole domain is divided into N_z number of grid points, then $l = k = 0,\ldots,N_z-1$. In order to satisfy the BC, Equation (6) can be incorporated to PWE of (5) with fields approximated as in (17). Assume $BC_{k,l}$ to be resultant BC matrix, that is given by,

$$\begin{aligned}\left[\alpha_1(x)\Omega_l^{0,1}|_{z=0} - \alpha_2(x)\delta_{k,l}|_{z=0}\right]\{a_l(x)\} &= 0,\\ [BC_{k,l}]\{a_l(x)\} &= 0.\end{aligned} \tag{20}$$

Combining (20) with (19) gives us the required system of linear equations that satisfy both the PWE and its boundary conditions.

$$[\delta_{k,l}]\{a_l'(x)\} + [L_{k,l} + S_{k,l} + BC_{k,l}]\{a_l(x)\} = 0 \tag{21}$$

Finally, the resultant linear system given in (21) is solved using CN method. The general solution of Equation (21) can be written as,

$$\{a_l(x+\Delta x)\} = \left(\frac{2[I_{k,l}] - \Delta x\,[L_{k,l} + S_{k,l} + BC_{k,l}]}{2[I_{k,l}] + \Delta x\,[L_{k,l} + S_{k,l} + BC_{k,l}]}\right)\{a_l(x)\}. \tag{22}$$

It is an iteractive algorithm. Once the system is initiated with starting field, field at the next range step can be calculated from the previous one. It is an unconditionally stable, a second order accurate system in range operator. The accuracy of height operator is dependent on the choice of wavelet Genus. Higher order wavelet provides higher accuracy. Overall complexity of algorithm is same as conventional finite methods. Although, CN Method provides fast solutions but the step-size should be chosen as small as necessary to overcome numerical oscillation problems [8].

4. NUMERICAL IMPLEMENTATION

Connection Coefficients derived by the Latto et al. [23] are for unbounded intervals. In order to deal with bounded intervals, fictitious domain method and capacitance matrix method are more common [10, 15]. However, Green function solution is required for the implementation of capacitance matrix method. But Green function is not readily known for PWE [25]. Due to this, fictitious domain approach is used to handle boundary condition in the solution of PWE. In this approach, interval is modified by adding a fictitious interval outside of interested domain. Same connection coefficient can be used to handle real boundary conditions as calculated by Latto et al.

4.1. Fictitious Domain Method

For the case of PWE, overall scenario is illustrated in Figure 3. Bottom surface ($Z_{\min}$) is finitely conductive surface while an absorbing layer is placed at the top (Z_{req}) of 'domain of interest'. Total altitude is divided into N_z number of grid points, therefore, φ has analytical

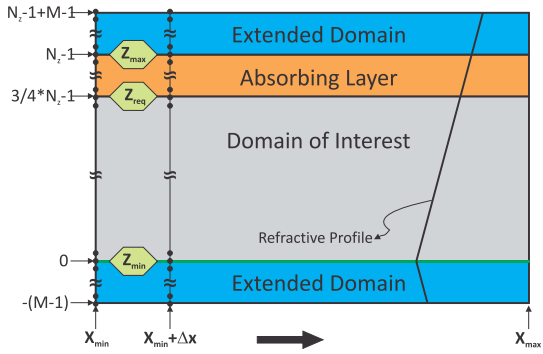

Figure 3. Computation domain for WGM.

boundaries at 0 and N_z-1. To satisfy the support of expansion in (17), i.e., $[-M+1, M-2+N_z]$, there is a need to add $M-1$ functions both at the top and bottom of 'domain of interest', where, M is the genus of wavelet scaling function. With this approach, the real domain will be stretched and analytical boundaries will be shifted to $-M+1$ and $M-2+N_z$. The dimensions of resultant linear system will be $N_z+2\times(M-1)-by-N_z+2\times(M-1)$. After discretizing with Daubechies-6 (D6), the matrices in (22) are obtained as:

$$S_{k,l}=\text{diag}\begin{bmatrix} S_{-5,-5} \\ \vdots \\ S_{0,0} \\ \vdots \\ S_{N_z-1,N_z-1} \\ \vdots \\ S_{N_z-1+5,N_z-1+5}\end{bmatrix},\quad BC_{k,l}=\text{diag}\begin{bmatrix} BC_{-5,-5} \\ \vdots \\ BC_{0,0} \\ \vdots \\ BC_{N_z-1,N_z-1} \\ \vdots \\ BC_{N_z-1+5,N_z-1+5}\end{bmatrix},$$

$L_{k,l}$ is a 9-diagonal matrix with $l=-4,\ldots,0,\ldots,4$,

$$L_{k,l}=\begin{bmatrix} \Omega_0^{0,2} & \Omega_1^{0,2} & \Omega_2^{0,2} & \ldots & \Omega_4^{0,2} & \ldots & 0 & \ldots & 0 & 0 & 0 \\ \Omega_{-1}^{0,2} & \Omega_0^{0,2} & \Omega_1^{0,2} & \ldots & \Omega_3^{0,2} & \ldots & 0 & \ldots & 0 & 0 & 0 \\ \vdots & \vdots & \vdots & \vdots & \vdots & \vdots & 0 & \vdots & \vdots & \vdots & \vdots \\ 0 & \Omega_{-4}^{0,2} & \Omega_{-3}^{0,2} & \ldots & \Omega_0^{0,2} & \ldots & 0 & \ldots & 0 & 0 & 0 \\ \vdots & \vdots & \vdots & \vdots & \vdots & \vdots & \vdots & \vdots & \vdots & \vdots & \vdots \\ 0 & 0 & 0 & 0 & 0 & \ldots & \Omega_0^{0,2} & \ldots & \Omega_3^{0,2} & \Omega_4^{0,2} & 0 \\ \vdots & \vdots & \vdots & \vdots & 0 & \ldots & \vdots & \vdots & \vdots & \vdots & \vdots \\ 0 & 0 & 0 & 0 & 0 & \ldots & \Omega_{-3}^{0,2} & \ldots & \Omega_{-1}^{0,2} & \Omega_0^{0,2} & \Omega_1^{0,2} \\ 0 & 0 & 0 & 0 & 0 & \ldots & \Omega_{-4}^{0,2} & \ldots & \Omega_{-2}^{0,2} & \Omega_{-1}^{0,2} & \Omega_0^{0,2} \end{bmatrix},$$

$$I_{k,l}=[\text{Identity}\quad\text{Matrix}]_{N_z+2(5)\times N_z+2(5)},$$

and

$$a_l(z)=\begin{bmatrix} a_{-5} & a_{-4} & \ldots & a_0 & \ldots & a_{N_z-1} & \ldots & a_{N_z-1+4} & a_{N_z-1+5}\end{bmatrix}^T.$$

A symmetric extension of refractive profile is taken in extended region at bottom while same profile is extended at top, as shown in Figure 3. We can write,

$$S_{-m,-m}=S_{m,m}\quad\text{for}\quad m=1,2,\ldots,5.$$

It can be seen that real boundaries exist at $BC_{0,0}$ and BC_{N_z-1,N_z-1}. It should also be noted that,

$$BC_{k,l}=0\ \text{ for }\ k,l\neq 0\ \&\ N_z-1.$$

For Dirichlet BC, coefficients $(a_l(z))$ should equal to zero at $Z_{\min}$. Hence, $[BC_{k,l}]$ and first M rows and columns of linear system, given in (22), will be zero. For Neumann BC, coefficients $(a_l(z))$ are unknown at $Z_{\min}$ but the implementation of Neumann BC will also yield $[BC_{k,l}] = 0$. For finitely conductive surfaces, an assumptions is made that the extended domain at bottom consists of the same material as at $BC_{0,0}$. We can write:

$$BC_{m,m} = \frac{-j}{2k_0}\alpha_2(x) \quad \text{for} \quad m = -5, -4, \ldots, 0.$$

After reaching the desired range step using marching solution given in (22), the required coefficients, $[a_0, \ldots, a_{N_z-1}]^T$, will be extracted from the extended domain solution.

4.2. Propagation Loss

In rectangular coordinate system, propagation factor can be calculated by

$$F = \sqrt{x}|u(x, z)|$$

where, x and z is in meters. x is the distance between the transmitting antenna and receiving antenna, and z is the altitude measured with respect to the mean sea surface. Once propagation factor F is obtained, the propagation loss in dB is determined by the basic radio wave theory in the form of [26],

$$L = L_f - 20\log F$$

where, L_f is free space propagation loss and computed from the formula given by,

$$L_f = 20\log f(\text{MHz}) + 20\log x(\text{m}) - 27.56$$

5. NUMERICAL RESULTS

To validate the efficiency of proposed method, the propagation path loss is calculated for standard and ducting environment conditions. Normalized Gaussian antenna pattern is used for all simulations. The bottom boundary is assumed to be flat sea surface. The results from AREPS package are obtained with only PE mode and with same parameters.

5.1. Standard Environment

In the first case, path loss results for 50 km transmission range are obtained using WGM as shown in Figure 4(a). Horizontally polarized transmitter antenna height is chosen at 50 m above the ground level.

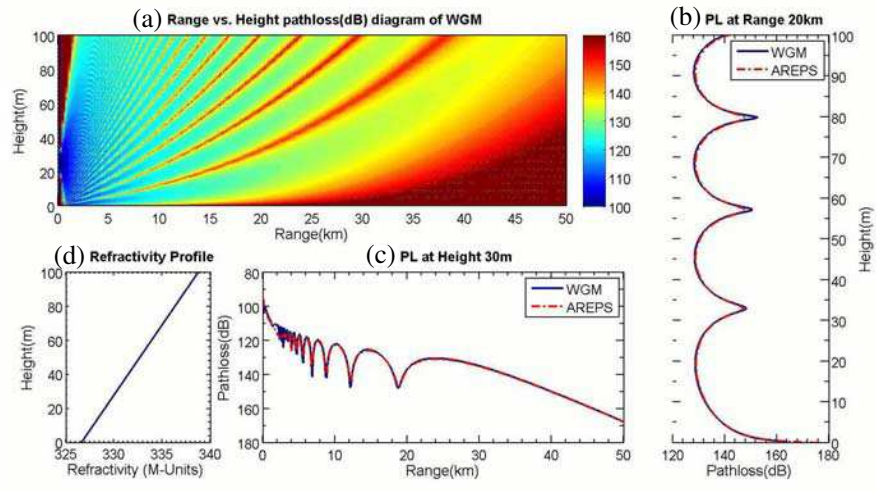

Figure 4. (a) Range (km) vs. height (m) pathloss (dB) diagram of WGM for standard environment. (b) Pathloss vs. height for range of 20 km. (c) Path-loss vs. range for height of 30 m. (d) Standard environment refractive profile.

Beam-width is set to be 3 degrees. Detailed comparison of results with AREPS package is illustrated in Figure 4(b)–(c). Figure 4(b) shows the comparison of pathloss versus height at range of 20 km while Figure 4(c) shows pathloss versus range comparison at the height of 15 m. It is observed that for normal gradient of refractivity, energy moves away from the earth's surface as shown in Figure 4(a). The results also show that for lower receiving antenna height pathloss is very high after a few kilometers . Communication range can only be improved by increasing the altitude of receiver and/or transmitter antenna.

5.2. Ducting Environment

Two different ducting environments are studied to validate the performance of WGM in ducting environment.

5.2.1. Surface Duct

To demonstrate the behavior of radiowave in surface duct, propagation loss is calculated with 5.8 GHz frequency. Simulations were performed with horizontally polarized antenna. Transmitter antenna is taken

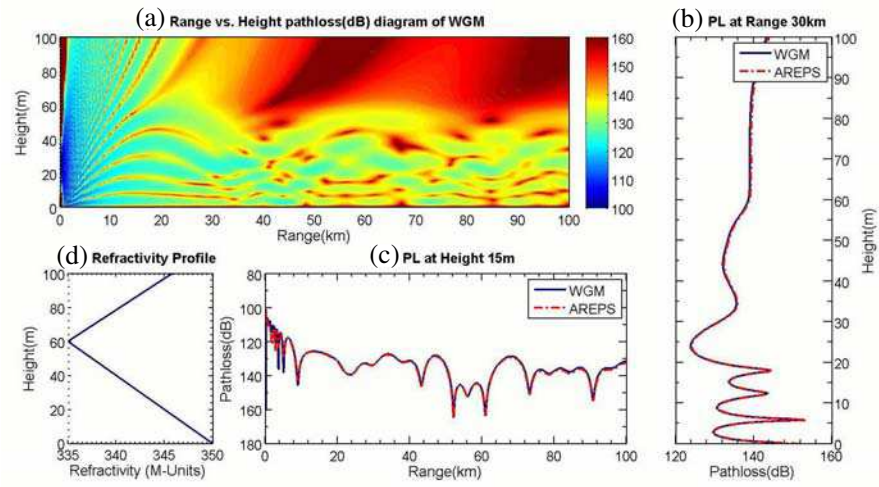

Figure 5. (a) Range (km) vs. height (m) pathloss (dB) diagram of WGM for surface duct. (b) Pathloss vs. height for range of 30 km. (c) Path-loss vs. range for height of 15 m. (d) Surface duct refractive profile.

at 25 m above the ground level. Beam-width is set to be 3 degrees. Anomalous radio wave propagation can be seen in Figure 5(a). Comparison of WGM results with AREPS is given in Figures 5(b)–(c). Ducting profile is illustrated in Figure 5(d). Result shows that propagation has been extended to several kilometers due to ducting phenomenon. As the total occurrence time of surface-based duct is very small, we cannot take benefit from this phenomenon for a reliable long range communication. But this phenomenon becomes a cause of strong interference to other communication systems even at far distances.

5.2.2. Evaporation Duct

Evaporation duct is one of the most important ducting phenomenon. 10.5 GHz is chosen for further path loss measurement because the effect of evaporation duct is more dominant in this range of frequencies. Simulations are carried out with horizontally polarized transmitter antenna with 15 m height above the ground level. Beam-width is set to be 2 degrees. Figure 6(a) shows the trapping of signals in evaporation duct. A detailed comparison of results with AREPS package is provided in Figures 6(b)–(c) for specific range and height. From results, it can be seen that in trapping condition, the signal attenuation is much less even at 100 km as shown in Figure 6(c).

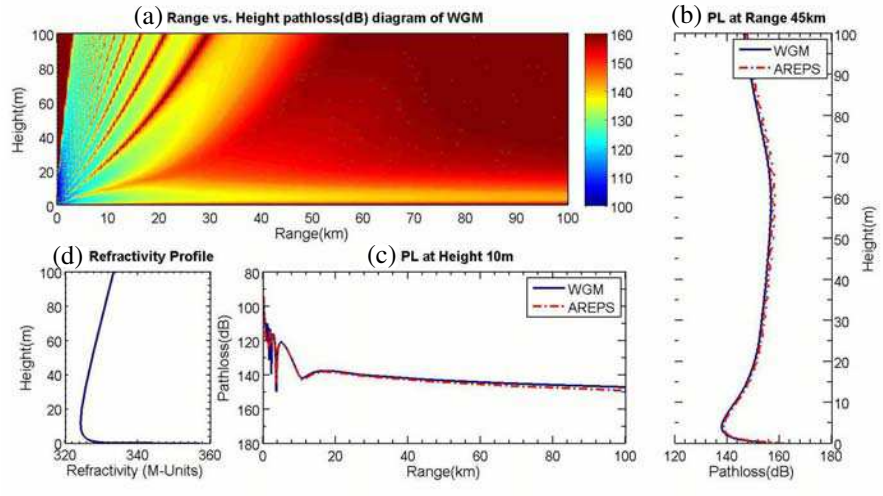

Figure 6. (a) Range (km) vs. height (m) pathloss (dB) diagram of WGM for evaporation duct. (b) Pathloss vs. height for range of 45 km. (c) Path-loss vs. range for height of 10 m. (d) Evaporation duct refractive profile.

Table 2. Mean relative squared error (MRSE) w.r.t. AREPS.

Environment Condition	Case	RMSE
Standard	Figure 4(b)	2.3128×10^{-5}
	Figure 4(c)	1.1456×10^{-4}
Surface Duct	Figure 5(b)	5.9757×10^{-6}
	Figure 5(c)	2.2107×10^{-4}
Evaporation Duct	Figure 6(b)	2.1279×10^{-5}
	Figure 6(c)	2.4398×10^{-4}

5.3. Discussion

In brief, the performance of WGM is measured under different complex environments and the accuracy of proposed method with respect to AREPS is summarized in Table 2. In Table 2, mean relative squared error (MRSE) is computed for the cases discussed in previous section. Table 2 shows that the maximum of mean squared relative difference of WGM and AREPS is of the order of 10^{-4}. Hence, results give a strong agreement with AREPS package. The formula used to calculate MRSE

is given by,

$$\text{MRSE} = \frac{1}{n}\sum_{i=0}^{k}\left(\frac{\text{AREPSdata}_i - \text{WGMdata}_i}{\text{AREPSdata}_i}\right)^2.$$

6. CONCLUSION

In this paper, a novel wavelet-Galerkin method is presented for the numerical solution of two dimensional parabolic equation. A new 'fictitious domain method' is also introduced for parabolic wave equation to incorporate the impedance boundary conditions. A brief discussion on the behavior of radiowave propagation in troposphere is also provided. At the end, results are compared with those from AREPS for both environment conditions — standard and ducting. The results show that the proposed algorithm is nearly as good as AREPS and it can be a better alternative to other well-known methods. From the simulation results, it is also found that the grid size for height and range operator is chosen carefully to make WGM computationally efficient. Smaller grid size is required for higher frequencies due to which WGM cannot save significant computation cost, relative to the AREPS. In spite of this, wavelet methods still have special properties like multi-resolution analysis and exact solution of connection coefficient which make them superior to other conventional methods and allow to provide higher accurate solutions.

REFERENCES

1. Levy, M., *Parabolic Equation Methods for Electromagnetic Wave Propagation*, Vol. 45, Inst. of Engineering & Technology, 2000.
2. Kuttler, J. and G. Dockery, "An improved-boundary algorithm for fourier split-step solutions of the parabolic wave equation," *IEEE Transactions on Antennas and Propagation*, Vol. 44, No. 12, 1592–1599, 1996.
3. Isaakidis, S. A. and T. D. Xenos, "Parabolic equation solution of tropospheric wave propagation using FEM," *Progress In Electromagnetics Research*, Vol. 49, 257–271, 2004.
4. Deshpande, V. and M. Deshpande, "Study of electromagnetic wave propagation through dielectric slab doped randomly with thin metallic wires using finite element method," *IEEE Microwave and Wireless Components Letters*, Vol. 15, No. 5, 306–308, 2005.

5. Oraizi, H. and S. Hosseinzadeh, "A novel marching algorithm for radio wave propagation modeling over rough surfaces," *Progress In Electromagnetics Research*, Vol. 57, 85–100, 2006.
6. Arshad, K., F. Katsriku, and A. Lasebae, "An investigation of wave propagation over irregular terrain and urban streets using finite elements," *World Scientific and Engineering Academy and Society (WSEAS)*, 105–110, 2007.
7. Apaydin, G. and L. Sevgi, "The split-step-fourier and finite-element-based parabolic-equation propagation-prediction tools: Canonical tests, systematic comparisons, and calibration," *IEEE Antennas and Propagation Magazine*, Vol. 52, No. 3, 66–79, 2010.
8. Apaydin, G. and L. Sevgi, "Numerical investigations of and path loss predictions for surface wave propagation over sea paths including hilly island transitions," *IEEE Transactions on Antennas and Propagation*, Vol. 58, No. 4, 1302–1314, 2010.
9. Barrios, A., "Considerations in the development of the advanced propagation model (APM) for us navy applications," *Proceedings of the International Radar Conference*, 77–82, Sep. 3–5, 2003.
10. Amaratunga, K., J. Williams, S. Qian, and J. Weiss, "Wavelet-Galerkin solutions for one dimensional partial differential equations," *International Journal for Numerical Methods in Engineering*, Vol. 37, No. 16, 2703–2716, 1994.
11. Liandrat, J., "Resolution of the 1D regularized burgers equation using a spatial wavelet approximation," *DTIC Document, Tech. Rep.*, 1990.
12. Qian, S. and J. Weiss, "Wavelets and the numerical solution of partial differential equations," *Journal of Computational Physics*, Vol. 106, No. 1, 155–175, 1993.
13. Pierce, I. and L. Watkins, "Modelling optical pulse propagation in nonlinear media using wavelets," *Proceedings of the IEEE-SP International Symposium on Time-Frequency and Time-Scale Analysis*, 361–363, Jun. 1996, 1996.
14. Reginska, T. and L. Eldn,"Solving the sideways heat equation by a wavelet-Galerkin method," *Inverse Problems*, Vol. 13, 1093, 1997.
15. Lu, D., T. Ohyoshi, and L. Zhu, "Treatment of boundary conditions in the application of wavelet-Galerkin method to an sh wave problem," *International Journal of the Society of Materials Engineering for Resources*, Vol. 5, No. 1, 15–25, 1997.
16. Gerstoft, P., L. Rogers, J. Krolik, and W. Hodgkiss, "Inversion for refractivity parameters from radar sea clutter," *Radio Science*, Vol. 38, No. 3, 122, 2003.

17. Barclay, L., *Propagation of Radiowaves*, Inst. of Engineering & Technology, 2003.
18. Hitney, H., J. Richter, R. Pappert, K. Anderson, and G. Baumgartner, Jr., "Tropospheric radio propagation assessment," *Proceedings of the IEEE*, Vol. 73, No. 2, 265–283, 1985.
19. Antoine, X., A. Arnold, C. Besse, M. Ehrhardt, and A. Schdle, "Review of transparent and artificial boundary conditions techniques for linear and nonlinear Schrödinger equations," *Communications in Computational Physics*, Vol. 4, No. 4, 729–796, 2008.
20. Daubechies, I., "Orthonormal bases of compactly supported wavelets," *Communications on Pure and Applied Mathematics*, Vol. 41, No. 7, 909–996, 1988.
21. Chui, C. K., *An Introduction to Wavelets*, C. K. Chui (ed.), Academic Press, 1992.
22. Restrepo, J. and G. Leaf, "Inner product computations using periodized daubechies wavelets," *International Journal for Numerical Methods in Engineering*, Vol. 40, No. 19, 3557–3578, 1997.
23. Latto, A., H. Resnikoff, and E. Tenenbaum, "The evaluation of connection coefficients of compactly supported wavelets," *Proceedings of the Princeton Conference on Wavelets and Turbulence*, 1991.
24. Beylkin, G., "On the representation of operators in bases of compactly supported wavelets," *SIAM Journal on Numerical Analysis*, Vol. 29, No. 6, 1716–1740, 1992.
25. Rino, C. L. and V. R. Kruger, "A comparison of forward-boundary-integral and parabolic-wave-equation propagation models," *IEEE Transactions on Antennas and Propagation*, Vol. 49, No. 4, 574–582, 2001.
26. Hitney, H. V., "Hybrid ray optics and parabolic equation methods for radar propagation modeling," *International Conference Radar*, 58–61, 1992.